Turbulent flow field in tangentially injected swirl flows in tubes

F. Chang and V. K. Dhir
Mechanical, Aerospace and Nuclear Engineering Department, School of Engineering and Applied Science, University of California–Los Angeles, Los Angeles, CA, USA

The turbulent flow field in a tube has been experimentally studied when fluid is injected tangentially. The experiments were conducted by injecting air through injectors placed on the periphery of an 88.9 mm inside diameter and 1.5 m-long acrylic tube. Four injectors of 15.88-mm inside diameter and six injectors of 22.23-mm inside diameter were used in the two sets of experiments. Tangential to total momentum flux rate ratio of 7.84 and 2.67 respectively were obtained in the two sets of experiments.

Using a single rotated straight hot wire and a single rotated slanted hot wire anemometer, profiles for mean velocities in the axial and tangential directions, as well as the Reynolds stresses were obtained. Axial velocity profile shows existence of a flow reversal region in the central portion of the tube and an increased axial velocity near the wall. Tangential velocity profiles have a local maximum, the location of which moves radially inwards with distance. Turbulence intensities are increased by swirl motion significantly due to the destabilizing distribution of angular momentum in the free vortex zone and the large shear stress near the boundary of the reversed flow. Reynolds stress data show an anisotropy in eddy viscosity. Turbulence energy and maximum axial velocity have been correlated with local swirl intensity.

Keywords: swirl flows; turbulence intensity; tangential injection

Introduction

A heat transfer enhancement concept in which swirl was introduced in the flow was proposed by Kreith and Margolis (1959). In this concept, part of the fluid enters axially while the remainder is injected tangentially at various locations along the tube axis. The radial pressure gradient results in thinning of the thermal boundary layer with an accompanying improvement in heat transfer. However, these authors never tested the concept. Hay and West (1975) measured local heat transfer coefficients and the flow field in a pipe at moderate Reynolds numbers (10,000 to 50,000) with tangential fluid injection from a single slot at the inlet. The heat transfer augmentation was found to be a function of the local swirl number, and a correlation for heat transfer was presented. Hay and West's results showed an increase of up to eightfold in local heat transfer.

Guo and Dhir (1987) studied the effects of injection-induced swirl on single- and two-phase heat transfer using water as the test fluid. They found a sixfold increase in the local single-phase heat transfer coefficient. The heat transfer coefficient was found to increase to a very large value just downstream of the injection location; then it decreased nearly exponentially with distance. On a constant pumping power basis, a net enhancement of about 20 percent could be achieved in their experiments. The ratio of the rate of the injected tangential momentum flux to the rate of axial momentum flux rather than Reynolds number was found to be the deciding factor in heat transfer augmentation.

Dhir and Chang (1992) experimentally studied the heat transfer enhancement in a tube by using tangential injection. The experiments were conducted with air as the test fluid. An enhancement of 35 to 40 percent on a constant pumping power basis was obtained with tangential injection. The increase in enhancement on a constant pumping power basis occurred because the authors used an injection manifold enclosed in a chamber. It was also found that the enhancement is strongly dependent on the ratio of tangential to axial momentum flux but is weakly dependent on Reynolds number. The authors also showed that tube diameter and number of injectors did not affect the heat transfer enhancement and as such were not independent parameters by themselves.

Several studies of turbulent flow field in decaying swirl flows have also been reported in the literature. The first experimental study in this area is that by Nissan and Bresan (1961). In their work, swirl flow was produced by tangentially injecting water into a tube through two ports placed diametrically opposite to each other. The ratio of tangential to axial momentum flux was approximately 8. Profiles of the static pressure along any radius of the tube always showed a minimum at the center, with a more or less steady increase towards the wall. The static pressure measured at the wall decreased steadily downstream from the inlet. The tangential velocity profile showed the velocity to increase from zero at the center to a maximum at a radius usually less than half the tube radius and to decrease again to be zero at the wall. The mean tangential velocity averaged over the cross section steadily decreased downstream

Address reprint requests to Professor Dhir at the Mechanical, Aerospace and Nuclear Engineering Department, School of Engineering and Applied Science, University of California–Los Angeles, Los Angeles, CA 90024.

Received 6 January 1994; accepted 22 May 1994

from the inlet. At low flow rate (Re $\leq$ 5,000), the axial velocity was forward throughout the tube. At higher flow rates, there was a flow reversal in the core of the tube. Under some circumstances, there was visual evidence of double reversal with water flowing forward near the wall and in the center and moving backwards in the intervening region. However, no velocity measurement for this flow pattern was shown in their work.

Ito et al. (1979) experimentally investigated the decay of swirl in the tangentially injected swirl flow. Water was used as the test fluid, and a very high value ($\sim$ 50) of the ratio of tangential to axial momentum flux was used. The tangential velocity distributions showed that there were two regions—a region of forced-vortex flow in the center of the tube and a surrounding region of so-called free-vortex flow. The swirl decayed with axial distance, and accordingly the extent of the region of solid rotational flow decreased. It was shown that the axial velocity was lower in the middle portion of the tube than near the wall, with a flow reversal region at the center. The radial velocity was much smaller than either the axial velocity or the tangential velocity, such that it could be ignored. The swirl intensity, defined as the circulation over a cross section, was found to decay exponentially with axial distance. It was found that the swirl decay behavior, as a function of the product of the dimensionless axial distance and reciprocal of Reynolds number based on the injection velocity, could be divided into two curves—one corresponding to the Reynolds numbers higher than 5,000 and one corresponding to the Reynolds numbers lower than 2,000.

Turbulence quantities in the confined swirl flow were measured by Weske and Sturov (1974) using a hot-wire anemometer. However, the swirl flow was produced by rotating a cylindrical chamber in which honeycombs and meshes were placed, resulting in the solid rotational flow at the inlet. Air was used as the test fluid, and the initial swirl intensity, defined as the ratio of the tangential velocity near the wall to the average axial velocity at the inlet, was below 3 in the experiments. They found that the maximum of the tangential velocity moved towards the center of the tube with axial distance from the inlet and that its magnitude gradually decreased. From their work, it was concluded that a large difference existed in the flow fields for high initial swirl intensity (higher than 2) and low initial swirl intensity (lower than 2). When the initial swirl intensity was less than 2, the axial velocity increased towards the center and reached a maximum at the center. In contrast, for the initial swirl intensity higher than 2, the axial velocity had a minimum at the center, increased towards the wall, reached a maximum and then decreased towards the wall. The drop in the velocity at the center persisted for up to about 50 tube diameters. However, the flow reversal was not found. For low initial swirl intensity (lower than 2), the swirl reduced the distance required for the profiles of turbulence intensity components to become fully developed. For high initial swirl intensity (higher than 2), the absolute values of all the components of Reynolds stresses increased steeply. The turbulence intensity components were increased by 3- to 5-fold in comparison to those in fully developed flow, and the maximum values were observed near the location where tangential velocity was maximum.

Kitoh (1991) experimentally studied confined swirl flow generated with guide vanes. The flow field was measured with X-wire anemometers. It was shown that the swirl intensity,

Notation

A	Cross-sectional area of the test section
a	Curve-fitting constant in Equation 2
A_j	Total cross-sectional area of all injectors
D	Inside diameter of the test section
D_j	Inside diameter of the injectors
E	Voltage response of the hot wire probe
E_0	Voltage respone of the hot wire probe at zero velocity
h	Pitch factor of the hot wire
k	Yaw factor of the hot wire
M_T	Total momentum flux rate of the axial flow
M_t	Tangential momentum flux rate of the injected fluid
$\dot{m}_T$	Total mass flow rate at the test section exit
$\dot{m}_t$	Mass flow rate of the injected fluid
$\overline{q^2}$	Twice energy of turbulence
$(\overline{q^2})_{av}$	Cross-sectional average value of twice energy of turbulence
R	Tube radius
r	Coordinate in the radial direction
r_{b1}	Radius of the boundary between the forced-vortex zone and transitional zone
r_{b2}	Radius of the boundary between the free-vortex zone and transitional zone
Re	Reynolds number
r_{fr}	Radius of the boundary of the reverse flow
r_{max}	Radius of the location of the peak tangential velocity
U	Mean axial velocity
u	Velocity fluctuation in the axial direction
$\overline{u^2}$	Mean square of velocity fluctuation in the axial direction
U_{av}	Bulk axial velocity
U_B	Velocity component normal to the plane of the prongs
U_c	Effective cooling velocity
$\overline{u_c^2}$	Mean square of effective cooling velocity fluctuation
U_N	Velocity component normal to the wire in the plane of the prongs
U_T	Velocity component tangential to the wire in the plane of the prongs
$\overline{uv}$	Reynolds stress component
$\overline{uw}$	Reynolds stress component
V	Mean radial velocity
v	Velocity fluctuation in the radial direction
$\overline{v^2}$	Mean square of velocity fluctuation in the radial direction
$\overline{vw}$	Reynolds stress component
W	Mean tangential velocity
w	Velocity fluctuation in the tangential direction
$\overline{w^2}$	Mean square of velocity fluctuation in the tangential direction
x	Coordinate in the axial direction

Greek symbols

α	Angle between the normal of the slanted wire and the probe axis
β	Angle of the flow direction
δ	Angle of rotation of the wire
η	Curve-fitting exponent in Equation 2
θ	Coordinate in the tangential direction
κ	Empirical constant in Equation 10
$(\nu_t)_{r\theta}$	Component of anisotropic eddy viscosity
$(\nu_t)_{xr}$	Component of anisotropic eddy viscosity
$(\nu_t)_{x\theta}$	Component of anisotropic eddy viscosity
ϕ	Angle between the flow direction and the normal to the wire

defined as a nondimensional angular momentum flux, i.e., the swirl number, decayed exponentially. The decay coefficients, however, were not constant but depended on the swirl intensity. The structure of the tangential velocity profile was classified into three regions: core, annular, and wall regions. The core region was characterized by a forced vortex motion, and the flow was dependent on the upstream conditions. In the annular region, the skewness of the velocity vector was noticeable and highly anisotropic, so the turbulent viscosity model did not work. In the wall region, the skewness of the flow became weak and a modified wall law was applicable.

Few authors report on the Reynolds stress components in the tangentially injected swirl flow with high swirl intensity. Swirl flow is characterized by anisotropy in eddy viscosity, in contrast to the k-ε model, which assumes the eddy viscosity to be isotropic. As suggested by Kobayashi and Yoda (1987), it is possible to predict the swirl flow field successfully by using a modified k-ε model with an anisotropic eddy viscosity. However, lack of systematic experimental data makes it difficult for any modeler to compare his/her results with actual data and thus improve the model to predict the swirl flow field in a pipe. Therefore, it is important to obtain systematic data including mean flow and Reynolds stresses. Furthermore, Reynolds stress data are useful in understanding the mechanisms of the heat transfer enhancement and the swirl decay.

In the present work, the decay of swirl in a tube subjected to tangential injection is investigated. Measurements of velocity profiles and Reynolds stresses in tangentially injected swirl flow are reported. Momentum flux ratios of 2.67 and 7.84 were chosen to study the effect of the initial swirl intensity.

Experimental apparatus and procedure

Figure 1 shows an experimental setup that was used to study the turbulent flow field in the tangentially injected swirl flow in a tube. The test section consists of a clear acrylic tube of 3.5 inch (88.9-mm) inside diameter, 0.125-inch (3.2-mm) wall thickness, and 1.5-m length. Air was injected tangentially through a set of tubular injectors. The injectors are made of tubing of the same material as the test section. Installation details of the tubular type of injectors are shown in Figure 2. Four injectors of 0.625-inch (15.88-mm) inside diameter and six injectors of 0.875-inch (22.23-mm) inside diameter were used in the two sets of experiments. Tangential to total momentum flux ratios of 7.84 and 2.67, respectively, were obtained in the two sets of experiments. The ratio 2.67 was chosen because, as shown by Dhir and Chang (1992), maximum enhancement in heat transfer on a constant pumping power is obtained with this ratio. The ratio 7.84 was employed to expand the data base, since most of the useable data reported in the literature have been obtained at momentum ratio less than 2.67. In the reported experiments, injectors were always placed near the tube inlet and air was used as the test fluid. The fluid entering tangentially was evenly distributed among the injectors and was controlled with float-type flow meters. The ratio of the momentum flux through the injectors to the total momentum flux through the test section is an important parameter and is defined as

$$\frac{M_t}{M_T} = \frac{\dot{m}_t^2}{\dot{m}_T^2}\frac{A}{A_j} \tag{1}$$

where $\dot{m}_t$ and $\dot{m}_T$ are the total mass flow rates through the injectors and the test section, respectively, and A and A_j are the cross-sectional area of the test section and the total area of the injectors, respectively. In the present work, all the fluid was injected tangentially; hence, the ratio $\dot{m}_t/\dot{m}_T$ is equal to unity.

Dantec 55P11 straight wire was used to measure the mean flow field of the injected swirl flow. The probe has a

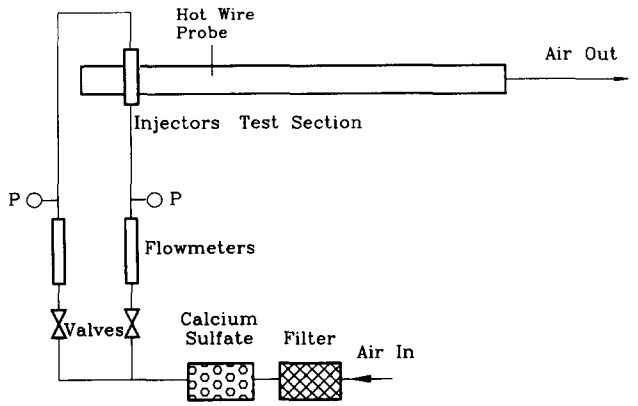

Figure 1 Schematic diagram of experimental apparatus

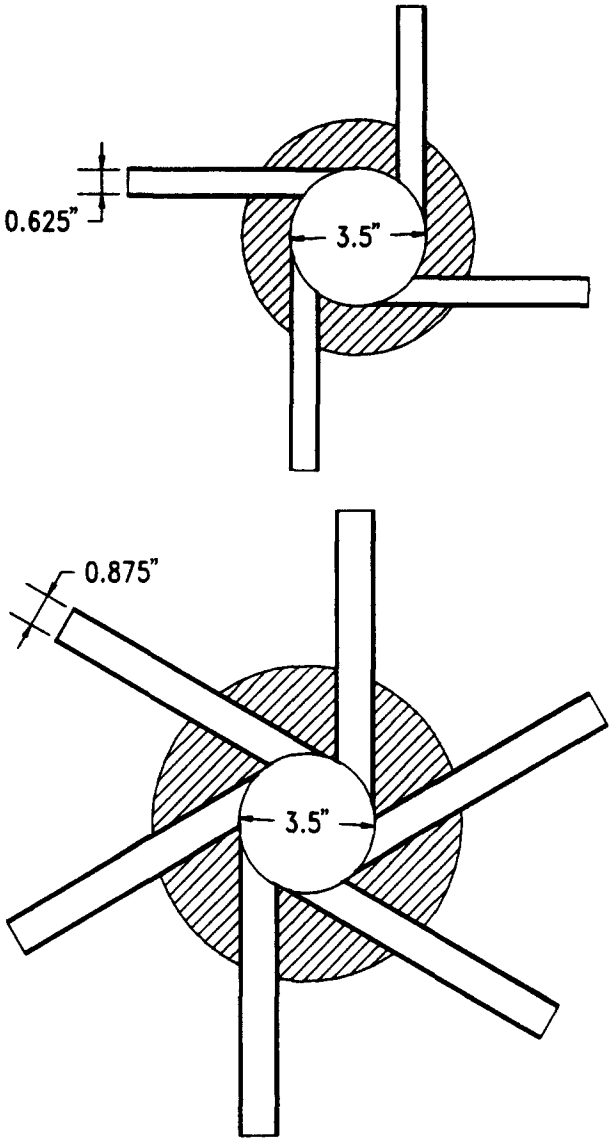

Figure 2 Details of injectors

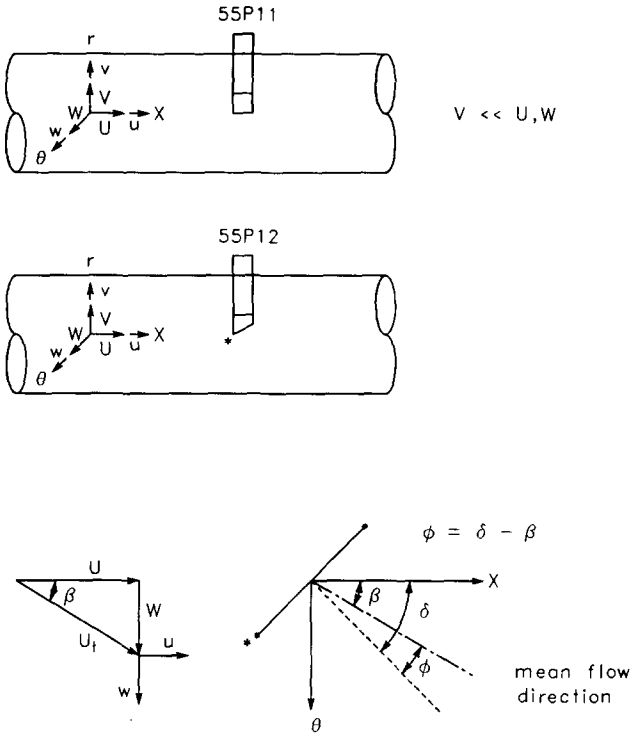

Figure 3 Orientation of Dantec 55P11 and 55P12 probes

platinum-plated 5 μm diameter tungsten wire perpendicular to the prongs. The probe is operated with a set of Dantec 56C01 constant temperature anemometers and 56C17 universal bridges. The probe support was aligned in the radial direction by a traversing mechanism from the mounting slot on the tube wall. The probe can be moved radially to the position where the measurements are to be made. The traversing mechanism can also rotate the probe over an angle ϕ about the mean flow direction, as shown in Figure 3. In the mean flow direction, the total velocity is perpendicular to the plane of the wire and the prongs, if it is assumed that the radial velocity is negligible. As such, the effective cooling velocity is maximum at that position. Thus from the probe output, the flow direction and the total velocity can be determined. Since the hot wire cannot sense the reverse flow, a total pressure probe was used to estimate the approximate flow angle before hot-wire measurements were made. The whole traversing mechanism can be slid in the mounting slot so that the flow field at axial distances of 6–10 hydraulic diameters can be measured. The axial velocity obtained in this manner is estimated to be accurate to ± 7 percent of the bulk axial velocity, defined as the average axial velocity over the cross section, while the tangential velocity is accurate to ± 13 percent of the bulk axial velocity. For details, see Chang (1994).

For measurement of the turbulence quantities, a hot-wire method was chosen, which was proposed by Fujita and Kovasznay (1968) and later modified by Bissonnete and Mellor (1974). The experimental procedure was divided into two sets of measurements. First, a straight-wire probe (55P11) was placed in the flow as described above and rotated every two degrees approximately from $\phi = -20°$ to 20° to obtain experimental records of both the mean effective cooling velocity and the mean square of the fluctuating effective cooling velocity against the angle of rotation. Second, a 45° slanted-wire probe (55P12) was similarly introduced and rotated every five degrees approximately from $\phi = 0°$ to $-75°$, as also shown in Figure 3. The same variables were recorded in the same manner.

The probes were calibrated in the orientation in which the velocity is perpendicular to the wire and is in the plane of the wire and the prongs. The calibration data can be expressed as

$$U_c = \left(\frac{E^2 - E_0^2}{a}\right)^{1/n} \tag{2}$$

where U_c is the effective cooling velocity, E_0 is the voltage response at zero velocity, and a and η are the curve-fitting constants. The value of η is about 0.5. Jørgensen (1971) used the following expression to account for the yaw and pitch effects:

$$U_c^2 = U_N^2 + k^2 U_T^2 + h^2 U_B^2 \tag{3}$$

where U_N, U_T, and U_B are velocity components normal to the wire in the plane of the prongs, tangential to the wire in the plane of the prongs, and normal to the plane of the prongs, respectively. To calibrate the yaw and pitch effects, the calibration was also done in those orientations in which the velocities are perpendicular to the probe; the probe was rotated every 10° from $-90°$ to 40°. A constant pitch factor and a constant yaw factor were used in the range of the calibration, with an error of ± 3 percent in the cooling velocity.

After a first-order expansion, the mean square of the fluctuating effective cooling velocity for the straight-wire probe can be written as

$$\begin{aligned}\overline{u_c^2} = {} & \overline{u^{2*}}(k^2 \sin^2\phi + h^2 \cos^2\phi) \\ & + \overline{w^{2*}} \frac{(h^2 - k^2)^2 \sin^2\phi \cos^2\phi}{k^2 \sin^2\phi + h^2 \cos^2\phi} \\ & + \overline{uw}^*[2(h^2 - k^2) \sin\phi \cos\phi]\end{aligned} \tag{4}$$

where ϕ is the angle between the normal of the wire and the mean flow direction, as shown in Figure 3. Similarly, the mean square of the fluctuating effective cooling velocity for the slanted-wire probe can be written as

$$\begin{aligned}\overline{u_c^2} = {} & \overline{u^{2*}}[\sin^2\phi(\sin^2\alpha + k^2\cos^2\alpha) + h^2\cos^2\phi] \\ & + \overline{v^{2*}} \frac{(1 - k^2)^2 \sin^2\phi \sin^2\alpha \cos^2\alpha}{[\sin^2\phi(\sin^2\alpha + k^2\cos^2\alpha) + h^2\cos^2\phi]} \\ & + \overline{w^{2*}} \frac{[h^2 - (\sin^2\alpha + k^2\cos^2\alpha)]^2 \sin^2\phi\cos^2\phi}{[\sin^2\phi(\sin^2\alpha + k^2\cos^2\alpha) + h^2\cos^2\phi]} \\ & - \overline{uv}^*[2(1 - k^2)\sin\phi\sin\alpha\cos\alpha] - \overline{vw}^*[2(1 - k^2)] \\ & \times \frac{[h^2 - (\sin^2\alpha + k^2\cos^2\alpha)]^2 \sin^2\phi\cos\phi\sin\alpha\cos\alpha}{[\sin^2\phi(\sin^2\alpha + k^2\cos^2\alpha) + h^2\cos^2\phi]} \\ & + \overline{uw}^*2[h^2 - (\sin^2\alpha + k^2\cos^2\alpha)]\sin\phi\cos\phi\end{aligned} \tag{5}$$

where α is the angle between the normal of the slanted wire and the probe axis. For the 55P12 proble, α is 45°. The turbulence quantities with a superscript * are defined in a frame of reference aligned with the local mean velocity vector.

The quantities in the frame of reference fixed to the axis of the test section are thus given by

$$\begin{aligned}\overline{u^2} &= \overline{u^{2*}}\cos^2\beta + \overline{w^{2*}}\sin^2\beta - 2\overline{uw}^*\sin\beta\cos\beta \\ \overline{w^2} &= \overline{u^{2*}}\sin^2\beta + \overline{w^{2*}}\cos^2\beta + 2\overline{uw}^*\sin\beta\cos\beta \\ \overline{v^2} &= \overline{v^{2*}} \\ \overline{uv} &= \overline{uv}^*\cos\beta - \overline{vw}^*\sin\beta \\ \overline{vw} &= \overline{uv}^*\sin\beta + \overline{vw}^*\cos\beta \\ \overline{uw} &= (\overline{u^{2*}} - \overline{w^{2*}})\sin\beta\cos\beta + \overline{uw}^*(\cos^2\beta - \sin^2\beta)\end{aligned} \tag{6}$$

In the experiments, the straight-wire probe was first rotated every two degrees from $\phi = -20°$ to 20° to obtain

experimental records of the mean square of the fluctuating effective cooling velocity. Components $\overline{u^2}^*$, $\overline{w^2}^*$, and $\overline{uw}^*$ were obtained by a least-square fit of the experimental data with Equation 4. The slanted-wire probe was then rotated every five degrees from $\phi = -75°$ to 0° to obtain experimental records of the mean square of the fluctuating effective cooling velocity. Substituting components $\overline{u^2}^*$, $\overline{w^2}^*$, and $\overline{uw}^*$ into Equation 5, the remaining components $\overline{v^2}^*$, $\overline{uv}^*$, and $\overline{vw}^*$ were computed by a similar technique using the experimental records of the slanted-wire probe. The range for the slanted-wire to rotate was chosen so that the singularity in solving for the three components could be avoided.

Discussion of results

Mean velocity distributions

Figure 4 shows the profiles of tangential mean velocity at various axial locations for initial momentum flux ratios of 7.84 and 2.67 and for $x/D \leq 10$. The tangential velocity increases with radius in the core region and reaches a peak value at $r/R = 0.4$–0.7; thereafter, it decreases with radius. By identifying the location at which the maximum tangential velocity occurs, the tangential velocity profile can be divided into two regions—the core and annular regions. The core and annular regions are characterized by forced-vortex- and free-vortex-type velocity distributions, respectively, as shown in Figure 5. However, there is a fairly large transition zone between the forced-vortex zone and the free-vortex zone. Near the wall, the tangential velocity reaches zero very rapidly. Since measurements could not be made very near the wall, the extent of the wall region identified in Figure 5 is somewhat arbitrary. The peak tangential velocity decreases with the axial distance from the injection location as a result of the swirl decay. The location where the tangential velocity is maximum moves towards the tube center with axial distance, i.e., the core region shrinks as swirl decays.

The profiles of the axial mean velocity are plotted in Figure 6. The data show a low velocity in the core region surrounded by a high-velocity annular region. Reverse flow appears in the central region, and the magnitude of the reverse flow and the area occupied by it decrease as swirl decays. The flow rate calculated by integrating the axial velocity profile over the cross section is within ±8 percent of the flow rate obtained from the flow meters. It is seen that for the same flow rate, higher maximum axial velocities occur as the momentum flux ratio is increased. With a knowledge of the axial variation of the axial velocity and by using the continuity equation, the radial

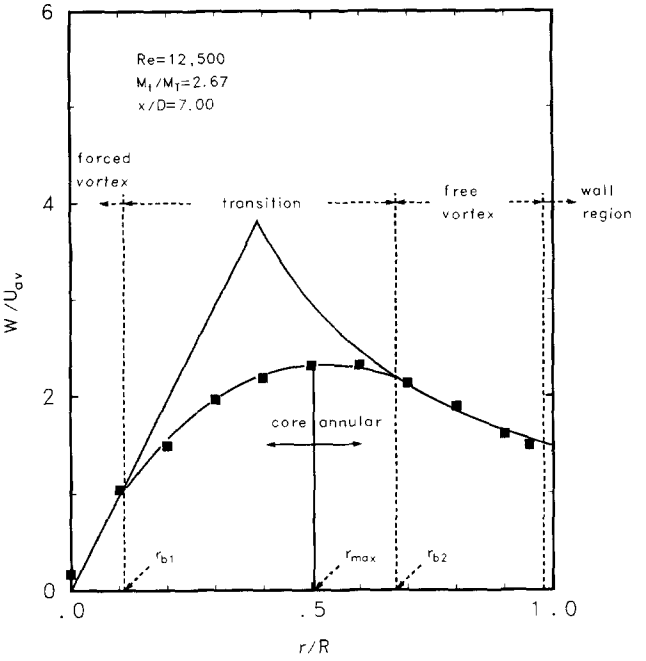

Figure 5 Forced vortex and free vortex

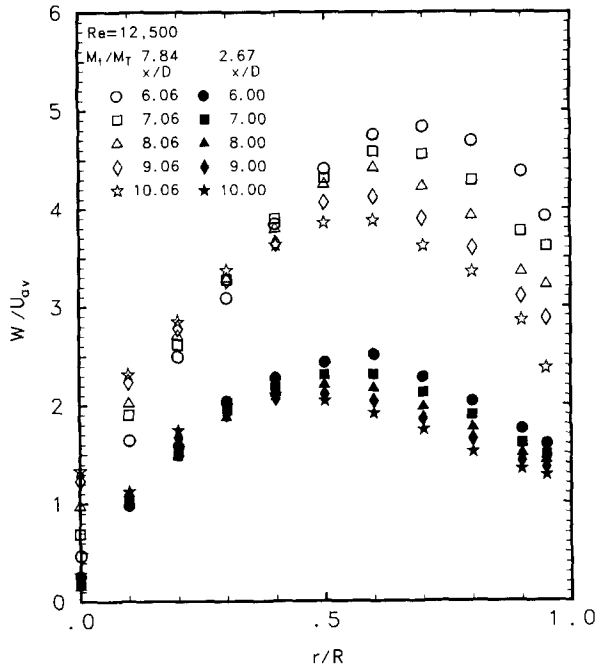

Figure 4 Tangential velocity profile

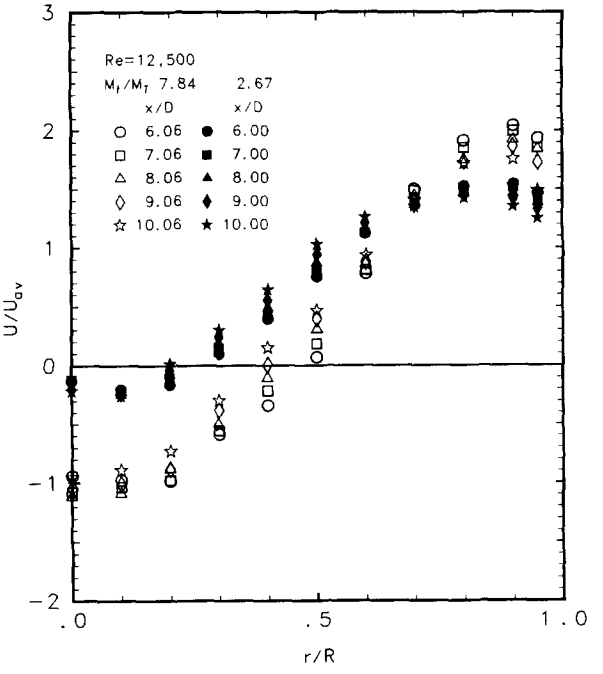

Figure 6 Axial velocity profile

velocity can be estimated. The radial velocity is obtained as

$$V = \frac{1}{r}\int_0^r \frac{\partial}{\partial x}(rU)\,dr \tag{7}$$

Figure 7 shows the radial velocity profiles. The maximum radial velocity is only 1.5 percent of the bulk axial velocity and occurs near the maximum of tangential velocity. It suggests that the mean flow is mostly two-dimensional (2-D) (x-θ plane).

The distribution of the static pressures is evaluated by substituting the tangential and axial velocities in the radial and axial momentum equations and by integrating these equations. The static pressure relative to the wall pressure at a reference location, i.e., at 10 hydraulic diameters from inlet, is plotted in Figure 8. The radial distribution of the static pressure shows that there exists an adverse pressure gradient in the core and a favorable pressure gradient near the wall. Adverse pressure gradient in the core corresponds to a reverse flow in the middle of the tube. As a result, for a given mass flow rate through the tube, the velocity in the forward direction increases in the outer region (near the wall). The friction factor based on either the wall pressure or the average static pressure over the cross section can be defined as

$$f = \frac{\dfrac{dP}{d(x/D)}}{\frac{1}{2}\rho U_{av}^2} \tag{8}$$

Figure 9 shows friction factors based on the wall pressure and the average static pressure. It is seen that the friction factor based on the wall pressure is much higher than that based on the average static pressure. This is due to the large radial pressure gradient that exists in the swirl flow.

For application purposes, it is important to determine the decay rate of the swirl intensity along the tube. The local swirl intensity, Ω, the ratio of rate of tangential to total momentum flux at a cross section, can be defined as

$$\Omega = \frac{2\pi\rho\int_0^R UWr\,dr}{\rho\pi R^2 U_{av}^2} \tag{9}$$

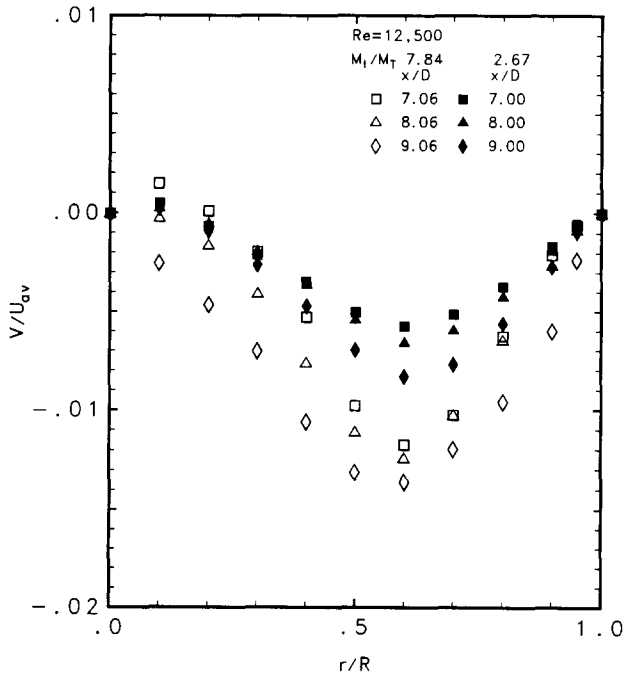

Figure 7 Radial velocity profile

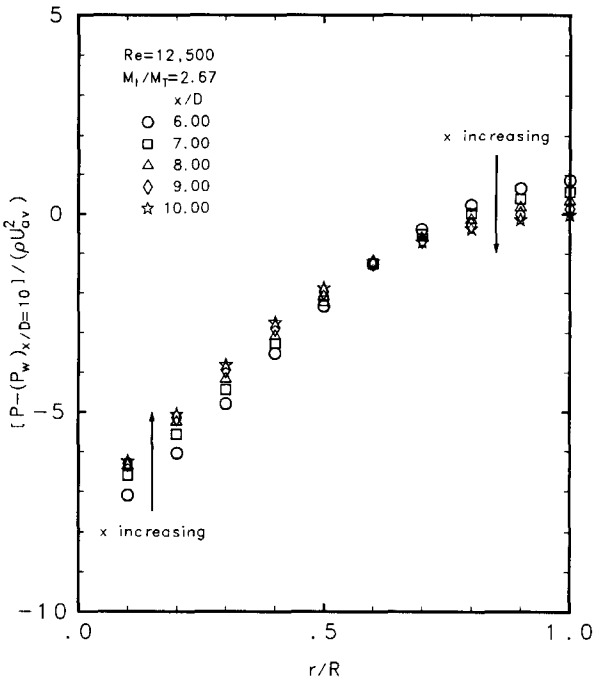

Figure 8 Static pressure

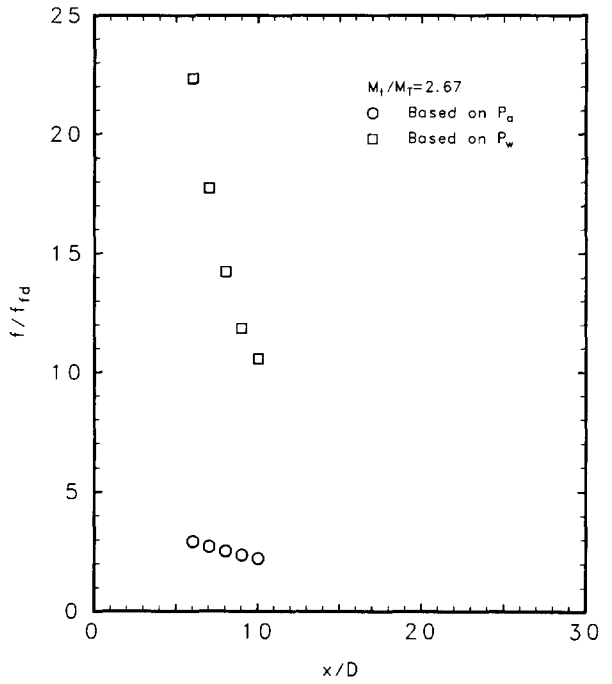

Figure 9 Friction factor

where U_{av} is the bulk axial velocity, R is the tube radius, and ρ is fluid density. The numerator in Equation 9 is the tangential momentum flux integrated over the cross section, while the denominator is the total momentum flux based on the bulk axial velocity. At the injection location, the local swirl intensity defined by Equation 9 should be equal to the initial momentum flux ratio M_I/M_T defined by Equation 1 due to the conservation of momentum. It is seen in Figure 10 that the swirl intensity tends to approach the momentum ratio in the limit of $x/D \to 0$. The swirl intensity is higher for the higher initial momentum

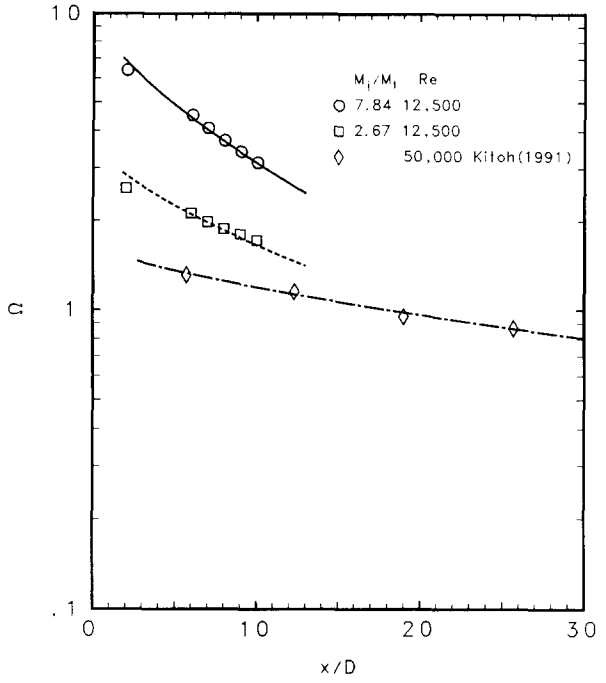

Figure 10 Swirl decay

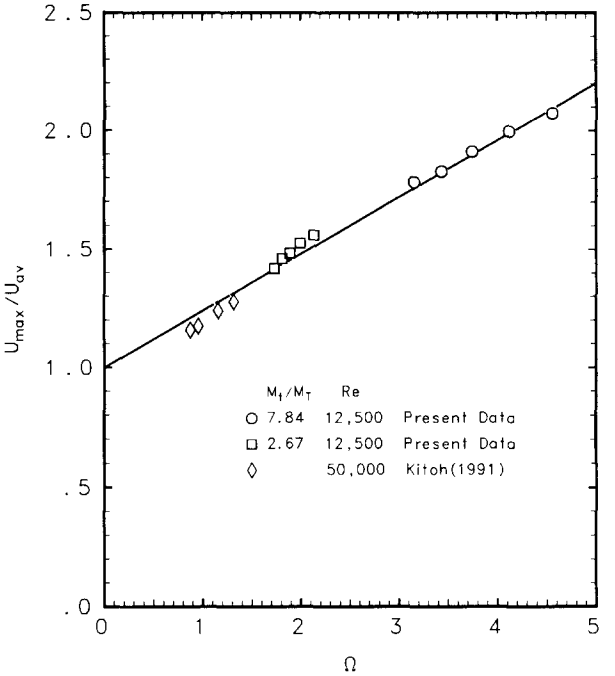

Figure 11 Maximum axial velocity

flux ratio, as is expected. Kitoh's (1991) data are also included in Figure 10. In Kitoh's experiments, the swirl was generated by guide vanes instead of tangential injection, and smaller swirl intensities were studied. The present data as well as Kitoh's data show that the swirl intensity decays approximately exponentially with the axial distance. The ratio of the decay rate $-d\Omega/d(x/D)$ to the local swirl intensity as a function of the dimensionless axial distance can be correlated as $(x/D)^{-0.3}$. As a result, the local swirl intensity can be written as

$$\Omega = 1.48\left(\frac{M_t}{M_T}\right)^{0.93} \exp\left[-\kappa\left(\frac{x}{D}\right)^{0.7}\right], \qquad \text{for } x/D \geq 2 \tag{10}$$

where

$$\kappa = 0.113\left(\frac{M_t}{M_T}\right)^{0.35} \tag{11}$$

The predictions from Equation 10 are also plotted in Figure 10. The behavior of the swirl decay is similar to the decay of the local heat transfer enhancement (Dhir and Chang 1992) with the axial distance. However, for the axial distance very close to the injection location ($x/D \leq 2$), the swirl appears to decay at a much slower rate, and thus the swirl intensity is nearly constant over a small distance downstream of the injection location. The existence of the reverse flow was found at all the measuring cross sections, including the cross section at two hydraulic diameters from the injection location. Vortex breakdown, which refers to a vortex core that undergoes an abrupt deceleration and forms a stagnation point followed by a region of flow reversal, was not identified at any of the measuring cross sections. With an increase of the swirl intensity, the vortex breakdown has generally been observed to migrate upstream toward the inlet (Faler and Leibovich 1977). Therefore, in the present high-swirl-intensity experiments, the vortex breakdown could have occurred near the injection location ($x/D \leq 2$). The slow decay of swirl over a small distance downstream of the injection location might be associated with the vortex breakdown phenomenon.

The maximum axial velocity occurred near the wall. As the swirl decays, the maximum axial velocity near the wall decreases. The maximum velocity in swirl flow is plotted as a function of swirl intensity in Figure 11. It is noticed that there is an almost linear relationship between the maximum velocity and the local swirl intensity with a very minor effect of the initial swirl. Higher swirl intensity results in a higher maximum axial velocity near the wall. The maximum axial velocity can be correlated as

$$\frac{U_{max}}{U_{av}} = 1 + 0.24\Omega \tag{12}$$

The radius, r_{fr}, of the reverse flow boundary can be plotted as a function of the swirl intensity. As shown in Figure 12, the flow-reversal region diminishes as the swirl intensity decreases. The data obtained at several axial positions for different initial swirl intensities appear to fall on a single curve and can be correlated as

$$r_{fr} = 0.174\Omega^{0.63} \tag{13}$$

The radius of the location of the maximum tangential velocity, r_{max}, as a function of the swirl intensity is also plotted in Figure 12. It can be seen that the location of the maximum tangential velocity moves towards the tube center when the swirl intensity decreases. The location of the maximum tangential velocity is found to be related to the swirl intensity as

$$r_{max} = 0.357\Omega^{0.44} \tag{14}$$

The boundary r_{b1} between the forced-vortex zone and the transition zone and the boundary r_{b2} between the free-vortex zone and the transition zone are plotted in Figure 13 as a function of the swirl intensity. The forced-vortex zone shrinks while the free-vortex zone stays fairly constant as the swirl intensity decreases. As a result, the transition zone expands with decrease in swirl intensity, i.e., the boundary between the core and the annular regions becomes more obscure as the swirl intensity becomes small.

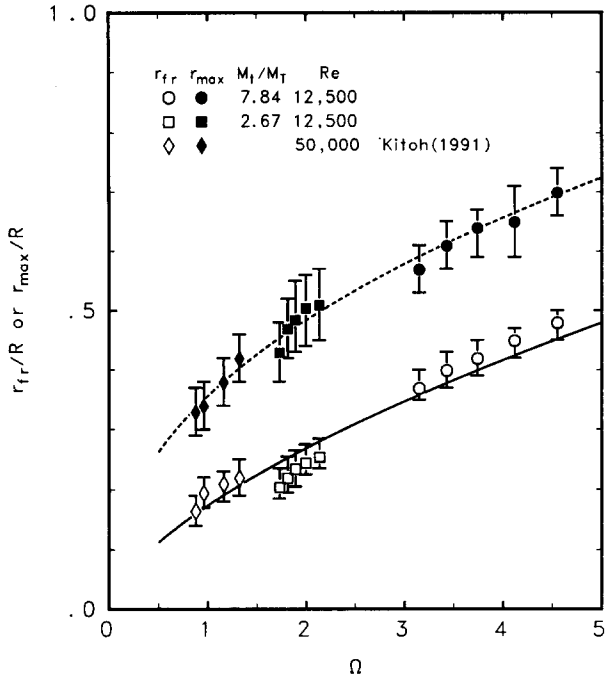

Figure 12 Boundary of flow reversal and location of maximum tangential velocity

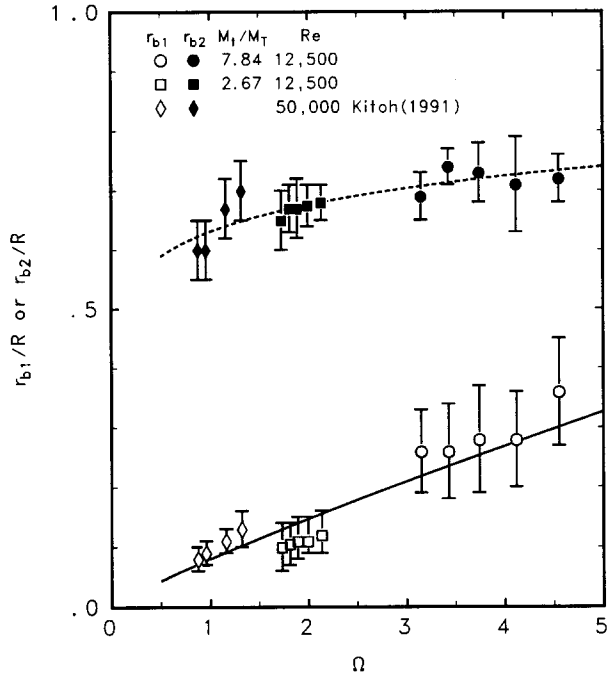

Figure 13 Boundaries of the transitional zone

Turbulence measurements

The radial distribution of turbulence intensities, $\overline{u^2}^{1/2}$, $\overline{v^2}^{1/2}$, and $\overline{w^2}^{1/2}$, normalized with the bulk axial velocity at various axial distances from the injection location, are shown in Figure 14. The data show that turbulence intensities have relatively large magnitude in swirl flow. The turbulence intensities are about 15 to 40 percent of the bulk axial velocity depending on the swirl intensity. It should be noted that the turbulent intensities are less than 10 to 15 percent of the local tangential velocity

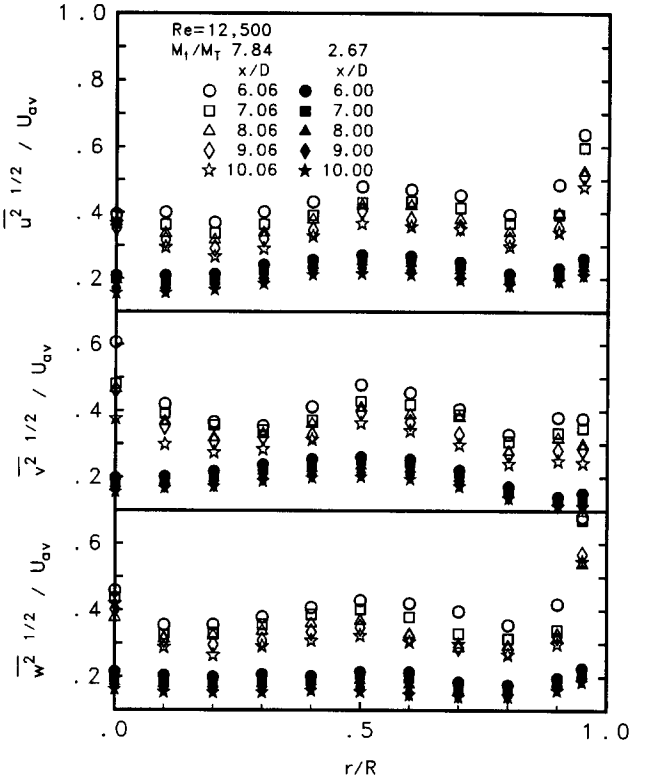

Figure 14 Turbulence intensities

or resultant velocity of the flow. As such, the linearization carried out in evaluating the intensities is considered to be valid. Turbulence intensities have similar profiles, i.e., there is a local maximum at about half the radius, which is close to the boundary of the flow reversal region, and a high value near the wall, except for $\overline{v^2}^{1/2}$, due to the turbulence-energy production from the wall shear stress. As a result of the radial diffusion of the turbulence energy, the profiles of turbulence intensity become flatter with axial distance. As such, turbulence intensities decrease as swirl decays. The root-mean-square value of the twice energy of turbulence, $\overline{q^2}^{1/2}$, is defined as

$$\overline{q^2}^{1/2} = (\overline{u^2} + \overline{v^2} + \overline{w^2})^{1/2} \tag{15}$$

The level of the turbulence intensity at a cross section can be represented by the cross-sectional average root-mean-square value of twice the energy of turbulence, defined as

$$(\overline{q^2})^{1/2}_{av} = \left(\frac{\int_0^R \overline{q^2} 2\pi r dr}{\pi R^2}\right)^{1/2} \tag{16}$$

The turbulence appears to be promoted significantly by the addition of the swirl flow, and this phenomenon seems to be caused chiefly by turbulence production from the radial gradient of the tangential velocity. It is reasonable to assume that the average intensity of turbulence over the cross section is closely related to the intensity of swirl. Figure 15 shows the relationship between the swirl intensity and the cross-sectional average root-mean-square value of twice the kinetic energy of turbulence, along with the data for the purely axial flow and Kitoh's data for lower swirl intensity. A linear relation appears to exist between cross-sectionally average turbulence intensity and local swirl intensity as long as $\Omega > 1$. This relation can be written as

$$(\overline{q^2})^{1/2}_{av} = 0.012 + 0.17\Omega \tag{17}$$

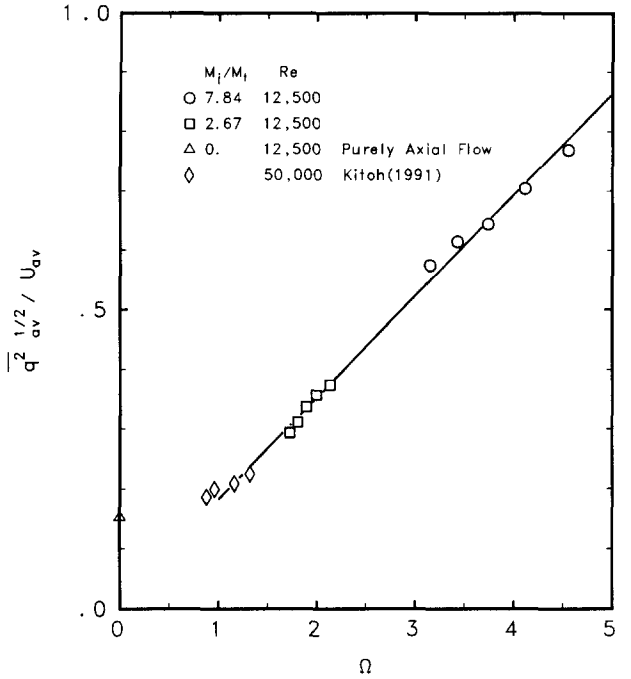

Figure 15 Relationship between swirl intensity and turbulence intensity level

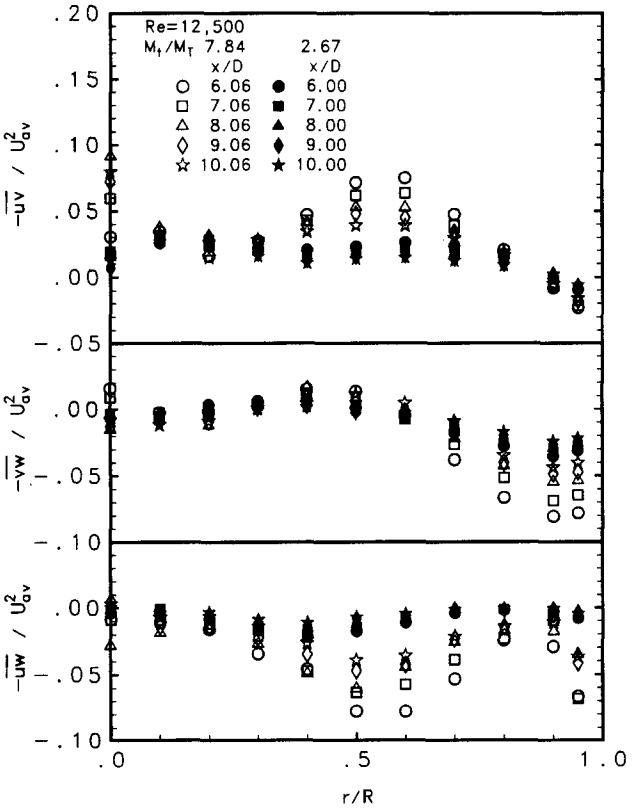

Figure 16 Reynolds stress components

The distribution of the Reynolds stress components $-\overline{uv}$, $-\overline{vw}$, and $-\overline{uw}$ over the cross section is shown in Figure 16. As seen in Figure 16, the Reynolds stress component $-\overline{uv}$ is negative near the wall, where the flow slows down, but positive in the central portion of the tube, where the axial velocity increases in the forward direction. In both regions, the magnitude of $-\overline{uv}$ decreases as swirl decays. The Reynolds stress component $-\overline{vw}$ is negative and large in the annular region, while it is small and sometimes positive in the core region, where the fluid rotates like a rigid body. As swirl decays, the magnitude of $-\overline{vw}$ in the annular region decreases. The value of $\overline{uw}$ should be predominantly positive, since angular momentum is transferred in the downstream direction. Figure 16 shows that in the region $0.3 < r/R < 0.7$, $\overline{uw}$ has a large positive value, while in the region $0.6 < r/R < 0.9$, small positive values of $\overline{uw}$ prevail. The magnitude of $\overline{uw}$ decreases as the swirl intensity decreases.

Using the measured Reynolds stress components, the eddy viscosities $(\nu_t)_{xr}$, $(\nu_t)_{r\theta}$, and $(\nu_t)_{x\theta}$ are calculated from the following relations:

$$(\nu_t)_{xr} = -\frac{\overline{uv}}{\partial U/\partial r}$$

$$(\nu_t)_{r\theta} = -\frac{\overline{vw}}{r\partial/\partial r(W/r)}$$

$$(\nu_t)_{x\theta} = -\frac{\overline{uw}}{\partial W/\partial x} \tag{18}$$

Figures 17, 18, and 19 show the eddy-viscosity distribution over the cross section. The data scatter widely when the gradients in the denominators are small and show dependence on the radial location. The large anisotropy among the three components can be seen by comparing the order of magnitude from Figures 17, 18, and 19. For example, for an initial momentum ratio of 7.84, the magnitude of $(\nu_t)_{x\theta}$ at $r/R = 0.7$ in the annular region is about 80 to 100 times the magnitude of $(\nu_t)_{r\theta}$ and about 20 to 40 times the magnitude of $(\nu_t)_{xr}$. This result is consistent with Kitoh's (1991) assertion with respect to the anisotropic nature of turbulent viscosity in the swirl flow. It is interesting to note that there exists a small region of negative eddy viscosities. Most of the negative values occur in the core region. Negative eddy viscosity implies that the mean

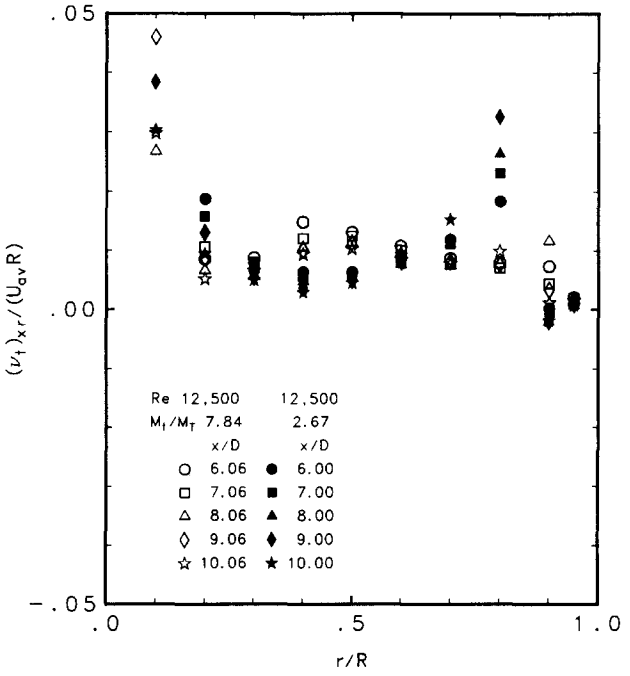

Figure 17 Eddy viscosity $(\nu_t)_{xr}$

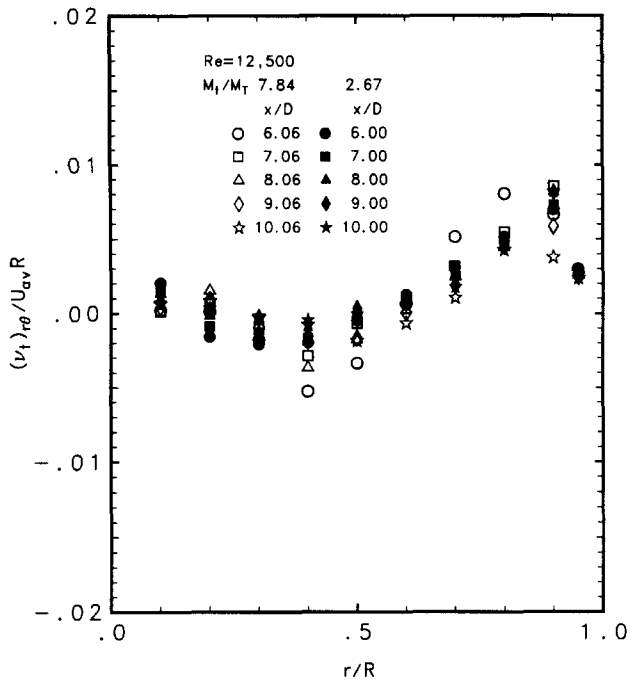

Figure 18 Eddy viscosity $(\nu_t)_{r\theta}$

momentum transport by turbulence is counter to the mean momentum gradient, i.e., negative turbulence energy production. The turbulence energy is extracted and fed back to the kinetic energy of the mean motion. This does not violate any basic principle and should not be particularly surprising. Hussain (1986) used coherent structure theory to explain negative turbulence production in shear flow. It is quite obvious that the isotropic eddy viscosity assumption is inappropriate for the swirl flow.

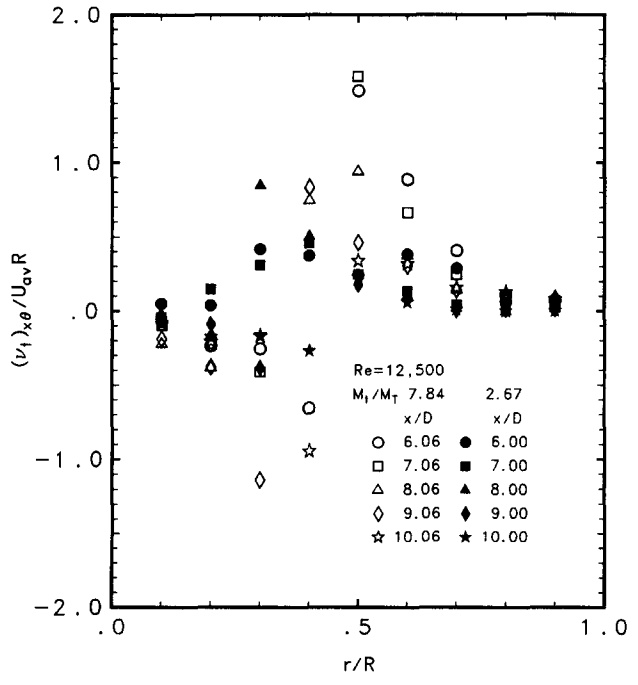

Figure 19 Eddy viscosity $(\nu_t)_{x\theta}$

The turbulence energy production can be obtained from Reynolds stress components and velocity gradients. There are only two significant terms: $-\overline{uv}\partial U/\partial r$ and $-\overline{vw}r\partial/\partial r(W/r)$. The first term exists in both axial flow and swirl flow, while the second term is the extra term due to the swirl motion. The turbulence production due to the radial gradient of the axial velocity is found to have high value near the wall and in the region close to the boundary between the forward and reverse flows. This indicates the existence of high shear near the wall and between two countercurrently flowing streams. The turbulence production from the radial gradient of the tangential velocity is dramatically increased (3 to 4 times the maximum turbulence production from the radial gradient of the axial velocity gradient) in the annular region where the tangential velocity decreases with the radius. This behavior can be explained from the Rayleigh instability criterion (Bradshaw 1973). If a fluid element in curved streamlines is disturbed in the radial direction, the displaced element will conserve its angular momentum about the center of curvature of the streamlines. Therefore, if the angular momentum numerically decreases outwards, as in the free-vortex zone, the displaced element will have a larger tangential velocity than its surroundings. As a result, the radial pressure gradient that maintains the mean flow in the circular path will not be able to keep the displaced element in equilibrium, and the displaced element will therefore continue to move outwards, i.e., the fluid motion will be unstable in this region. Conversely, if the angular momentum of the mean flow increases outwards, as in the forced-vortex zone, the radial pressure gradient will force the displaced element to return towards its original radius, about which it will oscillate. The same mechanism acts in a turbulent flow so as to transfer energy from the mean tangential velocity to the fluctuations.

The measured profiles of turbulence quantities and eddy viscosity can be used to develop correct numerical models for transport of momentum in swirl flows. The average turbulence energy and maximum axial velocity have been correlated with local swirl intensity, which in turn is related to the ratio of tangential to axial momentum flux. If enhancement in heat transfer is substantially attributed to increased axial velocity and increased level of turbulence, the dependence of heat transfer enhancement on the ratio of tangential to axial momentum flux can be explained from the present work.

Conclusions

1. From the tangential velocity profile, the swirl flow can be divided into a core region and an annular region. The core and annular regions are characterized by forced-vortex and free-vortex types, respectively. However, there is a fairly large transition zone between the forced-vortex zone and the free-vortex zone. This is consistent with earlier observations reported in the literature. The extent of core and annular regions have been correlated with local swirl intensity.
2. The swirl intensity decays as the axial distance from the injection location increases. As the swirl decays, the location of the maximum tangential velocity moves towards the tube center, which is consistent with the results from Ito et al. (1979).
3. The decay of swirl intensity has been correlated to the axial distance and the initial momentum flux ratio at a Reynolds number of 12,500.
4. A low axial velocity in the core region surrounded by a high-axial-velocity annular region is observed in the experiments. The maximum axial velocity near the wall decreases as swirl decays. A flow-reversal region is found in the core in

tangentially injected swirl flow. The area occupied by the flow-reversal region shrinks as the swirl intensity decreases.

5. The turbulence intensities are found to be 20 to 40 percent of the bulk axial velocity depending upon the swirl intensity in the tangentially injected swirl flow. The average intensity of turbulence over the cross section is found to vary linearly with the swirl intensity for $\Omega > 1$.
6. A large anisotropy among the three Reynolds stress components is observed. As an example, for the momentum flux ratio of 7.84, the magnitude of $(v_t)_{x\theta}$ is found to be about 80 to 100 times of the magnitude of $(v_t)_{r\theta}$ and about 20 to 40 times of the magnitude of $(v_t)_{xr}$ at $r/R = 0.7$ in the free-vortex region.
7. Negative eddy viscosities, i.e., negative turbulence productions, are observed in part of the core region.
8. The increase of the turbulence intensities is attributed to the destabilizing distribution of angular momentum in the free-vortex zone and the large shear stress near the boundary of the reversed flow.
9. Because of the dependence of turbulence intensities and maximum axial velocity on swirl intensity, the present work explains the augmentation of heat transfer with increase in ratio of tangential to axial momentum flux.

Acknowledgment

This work received support from Gas Research Institute under Contract No. 5086-260-1535.

References

Bissonnette, L. R. and Mellor, G. L. 1974. Experiments on the behavior of an axisymmetric turbulent boundary layer with a sudden circumferential strain. *J. Fluid Mech.*, **63**, 369–413

Bradshaw, P. 1973. Effects of streamline curvature on turbulent flow. AGARD-AG-169, NATO AGARD

Chang, F. 1994. Experimental and analytical study of heat transfer and flow field in tangentially injected swirl flow. Ph.D. dissertation, Mechanical, Aerospace and Nuclear Engineering Dept., University of California, Los Angeles

Dhir, V. K. and Chang, F. 1992. Heat transfer enhancement using tangential injection. *ASHRAE Trans.*, **98**, 383–390

Faler, J. H. and Leibovich, S. 1977. Disrupted states of vortex flow and vortex breakdown. *Phys. Fluids*, **20**, 1385–1400.

Fujita, H. and Kovasznay, L. S. G. 1968. Measurement of Reynolds stress by a single rotated hot wire anemometer. *Rev. Sci. Inst.*, **39**, 1351–1355

Guo, Z. and Dhir, V. K. 1987. Effect of injection induced swirl flow on single and two-phase heat transfer. *ASME HTD*, **81**, 77–84

Hay, N. and West, J. W. 1975. Heat transfer in free swirling flow in a pipe. *J. Heat Transfer*, **97**, 411–416

Hussain, A. K. M. F. 1986. Coherent structures and turbulence. *J. Fluid Mech.*, **173**, 303–356

Ito, S., Ogawa, K., and Kuroda, C. 1979. Decay process of swirling flow in a pipe. *Int. Chem. Eng.*, **19**, 600–605

Jørgensen, F. E. 1971. Directional sensitivity of wire and fiber-film: an experimental study. *DISA Inf.*, **11**, 31–37

Kitoh, O. 1991. Experimental study of turbulent swirling flow in a straight pipe. *J. Fluid Mech.*, **225**, 445–479

Kobayashi, T. and Yoda, M. 1987. Modified k-ε model for turbulent swirling flow in a straight pipe. *JSME Int. J.*, **30**, 66–71

Kreith, F. and Margolis, D. 1959. Heat transfer and friction in turbulent vortex flow. *Appl. Sci. Res.*, **8**, 457–473

Nissan, A. H. and Bresan, V. P. 1961. Swirling flow in cylinders. *A.I.Ch.E.J.*, **7**, 543–547

Weske, D. R. and Sturov, G. Ye. 1974. Experimental study of turbulent swirled flows in a cylindrical tube. *Fluid Mech. Sov. Res.*, **3**, 77–82